Plasma Sources Science and Technology

PAPER

Predictive, data-driven model for the anomalous electron collision frequency in a Hall effect thruster

To cite this article: Benjamin Jorns 2018 *Plasma Sources Sci. Technol.* **27** 104007

Plasma Sources Sci. Technol. **27** (2018) 104007 (14pp) https://doi.org/10.1088/1361-6595/aae472

Predictive, data-driven model for the anomalous electron collision frequency in a Hall effect thruster

Benjamin Jorns

Department of Aerospace Engineering, University of Michigan, Ann Arbor, MI 48109, United States of America

E-mail: bjorns@umich.edu

Received 8 July 2018, revised 30 August 2018
Accepted for publication 26 September 2018
Published 26 October 2018

Abstract

Symbolic regression is applied to find a data-driven model for the anomalous cross-field electron transport in a Hall effect thruster. This model is formulated in terms of an anomalous electron collision frequency that is related to the cross-field electron transport through a generalized Ohm's law. Empirically determined estimates of this anomalous collision frequency as a function of local plasma parameters from three 1–6 kW class Hall effect thrusters form the training dataset for this investigation. A commercially-available, evolutionary genetic algorithm is applied to regress this dataset and identify models for the anomalous collision frequency that are expressed as symbolic functions of the local plasma properties. It is found that these data-driven models not only fit the training dataset but that they can predict anomalous collision frequency values for a test dataset taken from a fourth thruster not used in the initial regression. Five existing models for the anomalous collision frequency derived from first-principles are applied to the same training and test datasets used for the data-driven model. The estimates of the anomalous collision frequency as a function of local plasma parameters from the data-driven models are shown to exhibit improved quantitative agreement with both datasets compared to the analytical models. These findings are discussed in terms of the physical insight they yield for identifying dominant physical processes that govern electron transport as well as the practical application of using this technique for creating predictive Hall thruster models.

Keywords: Hall thruster, modeling, cross-field transport, data-driven

1. Introduction

While the Hall effect thruster is one of the most successful and mature forms of electric propulsion flown to date, there are fundamental aspects of the operation of these devices that remain poorly understood (see [1]). Most notably, the electrons in these crossed-field devices behave non-classically, moving across their confining magnetic field lines at an anomalously high rate. The reason why this occurs is unknown, and this lack of understanding has been the major impediment to the development of self-consistent, predictive models for these devices.

Given the importance of numerical tools for Hall effect thruster analysis, qualification, and design, there has been a concerted effort over the past three decades to model self-consistently this anomalous effect. Direct numerical simulations based on a kinetic formulation offer the highest fidelity method for achieving this end [2–7]. However, kinetic approaches like particle-in-cell simulations are prohibitively expensive to computationally model faithfully the full-scale geometries of actual thrusters. Fluid-based and hybrid codes (kinetic ions and fluid electrons) offer reduced noise and faster computational times [8–17]. Yet, their use invites the question as to how to model correctly the anomalous electron transport in what is inherently a reduced fidelity framework. This poses a particular challenge in light of the fact that there is a growing body of evidence suggesting that the onset of the mechanism that drives the transport is kinetic [2, 18–22]. In order to use a fluid formulation self-consistently, it thus is critical to be able to find an approximate form for this anomalous effect that can be related to fluid-like parameters. This would allow the governing fluid equations to remain closed and therefore tractable.

There have been several attempts to arrive at this type of closed-form, fluid-based approximation for the anomalous electron transport. Proposed processes include enhanced collisionality through interactions with the walls [23, 24], Bohm diffusion [8], the influence of large-scale coherent structures [25, 26], and the onset of high-frequency turbulence [18–22]. To date, there has not been consensus about which process is dominant. Moreover, while there are ongoing efforts to incorporate closed-form approximations for the transport based on these proposed mechanisms in a fluid framework [23, 24, 27–31], success has been limited. The models will only match a subset of experimental data, only qualitatively capture trends in the electron transport, or in the extreme cases completely deviate from actual measurements. In light of these shortcomings and the growing demand for numerical thruster models, there thus remains a pressing need to find a functional, fluid-based expression for the electron transport.

Our approach in this investigation to this problem is a departure from previous works. While these earlier attempts focused on deriving a functional form from first-principles, we apply instead a data-driven, supervised machine learning (ML) approach. We use empirically determined estimates of the electron transport taken from a series of real Hall thrusters and apply symbolic regression to these datasets to identify a functional form for the dependence of the electron transport on background plasma parameters. This method is inspired by recent successful investigations performed in the computational fluid dynamics community to identify closures for approximating the effects of classical fluid turbulence [32, 33]. The potential advantage of this technique is that not only will it yield results that fit the data used to train it, but because the result is a symbolic expression, it may ultimately be extensible to new datasets (and therefore predictive).

With this approach in mind, this paper is organized in the following way. We describe in the first section our numerical methods. We outline a formulation for how to approximate the electron transport in a fluid hierarchy, detail the process for generating training datasets from experimental data by applying numerical inversion, and provide an overview of the numerical tool we employ for machine learning (ML) regression. In the second section, we present the results of the symbolic regression and examine the predictive capabilities of the data-driven models. We similarly compare the accuracy of these models to five leading models for anomalous electron transport that were derived from first principles. In the third and final section, we discuss the implications of our result in terms of the physical insight it offers, its limitations, and its potential use for developing predictive Hall thruster models.

2. Model description

2.1. Representing electron transport in a fluid framework

We describe in this section a fluid approach for describing the electron dynamics in a Hall effect thruster. Figure 1 shows the canonical geometry for this system in which an electric field, $\vec{E}$, is applied axially across a radially-confining magnetic

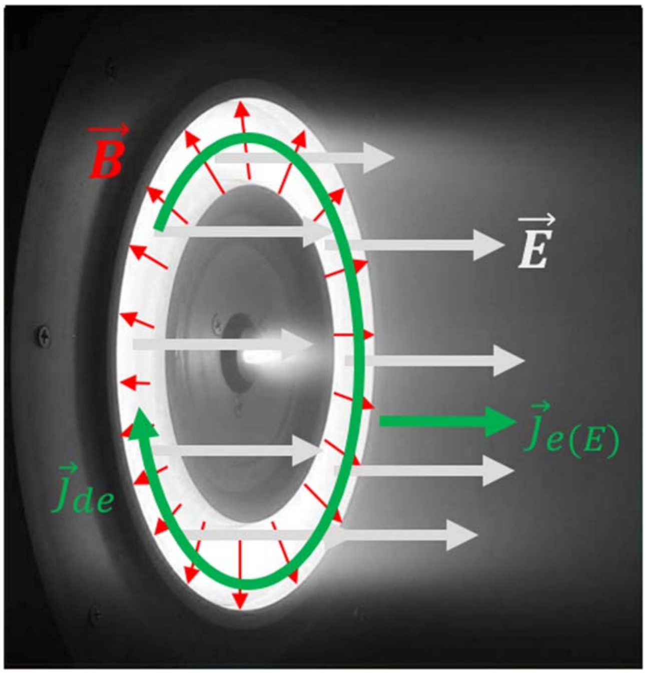

Figure 1. Canonical geometry for the Hall effect thruster with characteristic fields and electron current densities.

field, $\vec{B}$. This crossed-field configuration gives rise to a Hall effect electron current density in the azimuthal direction, $\vec{j}_{de}$. The cross-field electron current density, $\vec{j}_{e(E)}$, is parallel to the applied electric field.

We adopt a generalized Ohm's law to model the different components of the electron current density. Classically, this can be expressed as

$$\nu_e \frac{m_e}{q} \vec{j}_e = q n_e \vec{E} + \nabla P_e - \vec{j}_e \times \vec{B}, \quad (1)$$

where $\vec{j}_e = \vec{j}_{de} + \vec{j}_{e(E)}$ denotes the electron current density with components in both the cross-field and Hall directions, ν_e is the electron collision frequency including contributions from electron–ion and electron-neutral collisions, P_e is the electron pressure, q is fundamental charge, n_e is the electron density, and m_e is the electron mass. Physically, this expression represents a balance between driving forces (pressure gradients, electric field, and body force) with the drag on the electrons induced by collisions. In the classical fluid formulation, this Ohm's law is combined with energy and continuity equations for the electrons, ions, and neutrals (see [17]) to yield a closed set of equations for the fluid properties of each species (species temperature, T_s, drift velocity, $\vec{u}_s$, density, n_s, etc) that can be evaluated self-consistently in the Hall thruster geometry (figure 1). What has been found to date, however, is that numerical solutions with the classical formulation of equation (1) invariably yield predictions for the cross-field electron current, $\vec{j}_{e(E)}$, that are orders of magnitude too low compared to experimentally measured values (see [1] and references therein). This is the so-called problem of anomalous electron transport in these devices. The discrepancy between experiment and simulation suggests that this classical description may be missing physical processes that govern the electron dynamics. The challenge in modeling Hall effect thrusters with a fluid formulation is to find a way to represent these non-classical effects.

Fluid-based models of Hall effect thrusters currently resolve this issue by introducing new terms into the generalized Ohm's law (equation (1)) to drive higher cross-field current (see [29, 30, 34]):

$$\nu_e \frac{m_e}{q}\vec{\mathrm{j}}_e = qn_e\vec{E} + \nabla P_e - \vec{\mathrm{j}}_e \times \vec{B} + \vec{F}_{\mathrm{AN}}, \qquad (2)$$

where $\vec{F}_{\mathrm{AN}}$ is an 'anomalous' force density due to non-classical effects. Any components of this forcing term in the Hall direction in turn can promote cross-field electron current density through a body force. This forcing term alternatively can be formulated as an effective drag term, $\vec{F}_{\mathrm{AN}} = -n_e m_e\, \nu_{\mathrm{AN}} \vec{\mathrm{v}}_e$, where we have introduced an anomalous collision frequency ν_{AN} to represent the non-classical process. Couched in this form, equation (1) then becomes

$$(\nu_e + \nu_{\mathrm{AN}})\frac{m_e}{q}\vec{\mathrm{j}}_e = qn_e\vec{E} + \nabla P_e - \vec{\mathrm{j}}_e \times \vec{B}. \qquad (3)$$

This expression lends itself to an intuitive interpretation for how the anomalous effects promote cross-field transport. By making the typically valid assumption $\omega_{ce} \gg \nu_e + \nu_{\mathrm{AN}}$ for Hall thrusters where ω_{ce} is the electron cyclotron frequency, we can solve equation (3) for the direction of velocity parallel to the electric field to find

$$\vec{\mathrm{j}}_{e(E)} = \frac{q^2 n_e}{m_e}\frac{\nu_e + \nu_{\mathrm{AN}}}{\omega_{ce}^2}\left(\vec{E} + \frac{\nabla P_e}{qn_e}\right). \qquad (4)$$

This result shows that as the anomalous collision frequency increases, the magnitude of the cross-field transport is enhanced. The anomalous collisions thus have the same effect as classical collisions, helping to de-magnetize the electrons and thus cross the confining magnetic field.

We mention here that in the fluid modeling treatments of Hall effect thrusters, the problem also can be formulated in terms of anomalous mobility, μ_{AN}, in lieu of a collision frequency (see [28]). In the case of magnetized electrons ($\omega_{ce} \gg \nu_e + \nu_{\mathrm{AN}}$), it can be shown that this parameter scales linearly with the anomalous collision frequency, $\mu_{\mathrm{AN}} = \nu_{\mathrm{AN}}/(\omega_{ce} B)$. The anomalous mobility and collision frequency thus are effectively interchangeable when discussing the need to introduce new parameters to drive the cross-field current.

2.2. The problem of closure in a fluid framework

The major consequence of introducing an anomalous collision frequency (or mobility) into the electron Ohm's law (equation (3)) is that it opens the governing set of equations. Classically, in a Branginskii-like formulation for a low-temperature plasma, the fluid equations and transport coefficients (e.g. Coulomb collisions) are known and can be expressed as functions of typical fluid properties (T_s, $\vec{\mathrm{u}}_s$, n_s, …). The number of equations for the system matches the number of unknowns and is therefore numerically tractable. Introducing the additional unknown, ν_{AN}, in the Ohm's law invites the problem of closure. In order to be able to evaluate the modified set of fluid equations self-consistently, it is necessary to add another equation or find a way to relate this anomalous term back to the original set of properties solved for in the fluid equations, e.g. a functional form of the type $\nu_{\mathrm{AN}}(T_s,\ n_s,\ \ldots)$.

Table 1. Functional forms proposed for anomalous collision frequency in Hall effect thrusters. In these expressions, K, C, and α are scalar constants, $\vec{u}_i$ is ion drift in the axial direction, v_{de} is the electron drift in the Hall direction, and c_s denotes the ion sound speed.

Mechanism	ν_{AN}
Wall collisions	Kc_s
Bohm	$\frac{1}{16}\omega_{ce}$
Turbulence I	$\frac{1}{K}\omega_{ce}\left(\frac{\mathrm{v}_{de}}{c_s}\right)^2$
Turbulence II	$K\frac{\lvert\nabla\cdot(\vec{u}_i n_e T_e)\rvert}{m_e c_s n_e \mathrm{v}_{de}}$
Turbulence III	$\frac{1}{K}\omega_{ce}\left(\frac{1}{1+(C\,\nabla \mathrm{v}_{de})^{\alpha}}\right)$

To this end, previous attempts to close the electron transport equations for Hall effect thrusters have employed a first-principles approach. These rely on proposing a mechanism not included in a classical formulation, such as enhanced transport due to collisions with the walls of the thruster [35–37] or interactions with kinetically-driven microturbulence [28, 29, 38, 39], and making the ansatz that this process drives the anomalous transport. The impact of this mechanism on the electron dynamics is then translated via a first-principles derivation into an effective collision frequency that depends on fluid and thruster parameters. As a result, just as there is a closed-form expression for Coulomb collisions as a function of temperature and density found through first principles analysis, so too can the anomalous collision frequency be expressed as a function of fluid-properties, $\nu_{\mathrm{AN}}(T_s, n_s, \ldots)$. The key advantage of this technique is that the new, closed set of equations are in principle predictive, allowing for simulating new geometries and operating conditions.

We show in table 1 a list of five of the leading expressions for the electron collision frequency that have been identified to date for Hall effect thrusters from first-principles analysis.

In brief, these mechanisms assume that the anomalous electron dynamics are governed by enhanced collisionality due to electron interactions with the discharge chamber walls [24, 35–37, 40], Bohm diffusion [8], viscosity from a turbulent spectrum with its growth balanced by dissipation at small lengthscales (Turbulence I) [28], the electron cyclotron drift instability saturated by ion trapping and quasilinear deformation of the electron distribution function (Turbulence II) [29, 41], and shear-suppressed turbulence in the thruster (Turbulence III) [38]. These expressions in table 1 represent some of the most advanced attempts to approximate self-consistently the anomalous electron transport in fluid simulations of Hall effect thrusters. They have been employed in different measure to examine various aspects of thruster operation, and under certain circumstances, they have been able to yield numerical results that match thruster behavior. Increasingly sophisticated efforts in turn have employed combinations of these closures [11, 17, 42, 43] or have leveraged the insight from them to introduce additional governing equations for the collision frequency [30, 34]. With that said, despite the physical insight that has emerged from using these closures, they have had limited success in yielding fully predictive numerical simulations [23, 24, 27–31]. The thruster simulations employing these closures will only match a subset of experimental data, only qualitatively represent trends in the collision frequency, or in some cases, deviate entirely from actual measurements. In light of these limitations, we outline in the following section an alternative approach to this problem.

2.3. Regression to find a functional form for closure

Although from the perspective of fundamental understanding there is no substitute for a first-principles analysis, a data-driven model may offer a more expedient and practical alternative for closing the fluid equations for a Hall thruster. The central idea is that if we are able to generate a large, representative dataset of measurements of the anomalous collision frequency as a function of local plasma parameters in actual Hall thrusters, it may be possible to infer from regression, i.e. fitting the data, a functional form for the collision frequency. The resulting expression may or may not have direct physical meaning, but by design it will be able to capture trends in the dependence of the anomalous collision frequency on plasma parameters, $\nu_{\mathrm{AN}}(T_s,\ n_s,\ \ldots)$.

The ability to apply this data-driven approach is predicated on two requirements: the existence of large datasets of the anomalous collision frequency and the ability to regress this data rigorously. With respect to the first requirement, there are two paths for empirically determining the anomalous collision frequency in Hall thrusters: direct experimental measurement and numerical inversion. In the direct experimental approach, the Ohm's law approximation (equation (4)) is inverted to express the anomalous collision frequency as a function of local plasma parameters, e.g. electric field and electron current density. By measuring these plasma properties directly, it is in principle possible to calculate the anomalous collision frequency. While simple in concept, this direct measurement method to date has been nearly impossible to perform accurately and non-invasively. Indeed, despite ongoing efforts to improve upon experimental techniques [44–46], non-invasive measurements of the electron density and the cross-field electron current density have proved to be particularly challenging in these devices. The difficulty in characterizing these plasma properties, the uncertainty inherent to making this measurement, and the expense ultimately have limited the size of the available datasets.

Numerical inversion provides an alternative technique to overcome the challenges with direct experimental measurements of the anomalous collision frequency (see [17]). In this approach, the user considers an existing thruster configuration

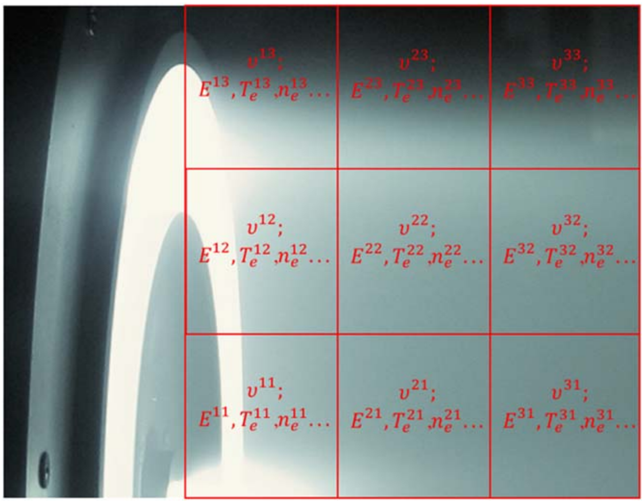

Figure 2. Side view of the upper half of a Hall effect accelerator with a sample mesh of data points where the anomalous collision frequency is specified by the user and plasma parameters such as electric field, density, and temperature are calculated.

with experimental measurements of key plasma properties that are more easily, non-invasively, and accurately characterized than the electron current density and plasma density. The axial component of the ion velocity along the thruster channel centerline is a common example. The user then builds a simulation of this thruster based on the standard fluid equations and an electron Ohm's law modified according to equation (3). We show in figure 2 an illustrative example of this: a 3×3 simulation mesh in the r-z domain applied to an existing thruster. Each mesh location is characterized by the standard fluid parameters (electric field, E^{11}, electron temperature, T_e^{11}, density, n_e^{11}, etc., where the upper index refers to the grid location) while the anomalous collision frequency at each mesh point, $\upsilon_{\mathrm{AN}}^{11}$, $\upsilon_{\mathrm{AN}}^{12}$, … , is left as a free input parameter specified by the user. The user closes the governing fluid equations by inputting fixed numerical values for the anomalous collision frequency at each mesh point, i.e. $\upsilon_{\mathrm{AN}}^{11} = c_{11}$, $\upsilon_{\mathrm{AN}}^{12} = c_{12}, \ldots, \upsilon_{\mathrm{AN}}^{33} = c_{33}$, where $c_{11}, c_{12}, \ldots, c_{33}$ are constants. With these values, the fluid equations can be solved to yield estimates of global parameters like thrust and discharge current as well as local plasma parameters like electron temperature and ion drift. The process of numerical inversion in this context is to find the values for the anomalous collision frequency at each grid point that when used in the governing equations allow the code to output plasma and thruster properties that match the experimental dataset.

In Hall thruster simulations, a common method for performing this numerical inversion relies on an iterative procedure (figure 3). The code user provides a numerical, fixed 'guess' for the anomalous collision frequency at each mesh point, and the numerical code is solved until it converges to a solution. The results of the code are then checked against experimental measurements from the actual thruster. If the measurements do not agree, the user iterates on the guess for the collision frequency and follows this process until agreement with experimental measurements is found.

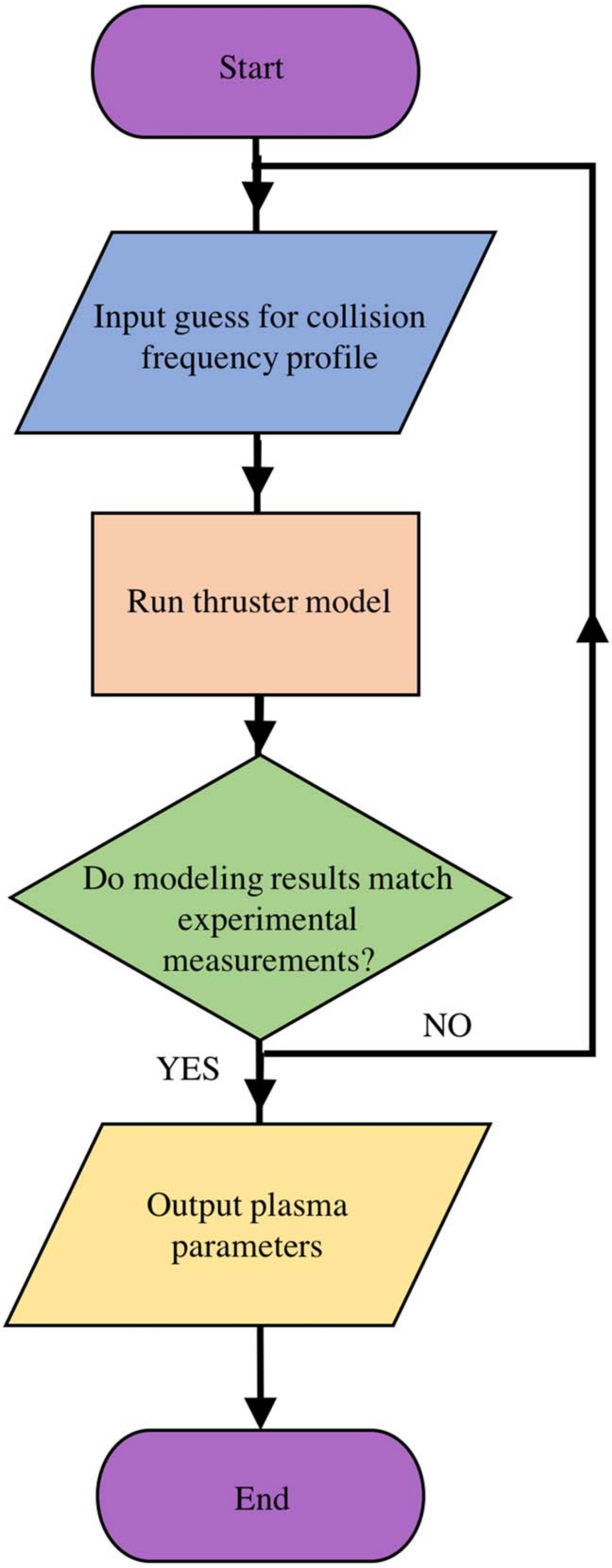

Figure 3. Flow chart for determining electron collision frequency profile through the process of numerical inversion.

Returning to the illustrative example in figure 2, the ultimate result of this iterative process would be a nine-component dataset with numerical values $S = \{((\upsilon_{\mathrm{AN}}^{11},\ T_e^{11},\ n_e^{11}, \ldots), ((\upsilon_{\mathrm{AN}}^{12},\ T_e^{12},\ n_e^{12}, \ldots), \ldots (\upsilon_{\mathrm{AN}}^{33},\ T_e^{33},\ n_e^{33}, \ldots)\}$. Here the value of the anomalous collision frequency at each mesh point determined from numerical inversion is identified with the local plasma properties output by the code at the same mesh point. In practice, the grids for numerical simulations are substantially larger than the illustrative example shown in figure 2, consisting of several thousand points. By considering multiple thrusters and multiple operating conditions, it thus is possible to build large-scale datasets of the measured anomalous collision frequency as a function of local plasma properties [11, 47, 48].

Armed with these datasets for the anomalous collision frequency, the second requirement for our proposed work is the ability to regress these data. The goal is to try to find a functional form, $\nu_{\mathrm{AN}}(T_e,\ n_e, \ldots)$, that depends on the plasma parameters and fits the experimental dataset. There are many types of regression that can be applied to this end. Traditionally, physical intuition or first-principles analysis guides the choice of a candidate function with unspecified coefficients as free parameters. For example, we may propose $\nu_{\mathrm{AN}} = c_1 T_e + c_2 (n_e)^2 + c_3 u_i$ as a potential function. We then would apply a least-squares analysis to the existing dataset, S, to determine the coefficients. The challenge with this traditional approach is that we do not know *a priori* the functional form that ν_{AN} should take for the Hall effect thruster. Moreover, it is prohibitively difficult to discern functional trends for this parameter, e.g. a linear dependence on temperature, just from inspection of the data—there are too many independent parameters. Indeed, in the extreme case, fluid codes for Hall effect thrusters that simulate electrons, neutrals, and multiple fluid ion species and charge states can have over 30 independent plasma parameters at each grid point [49]. The ability to mix, match, and explore systematically different combinations of functional forms that fit the local plasma parameters is with limited exceptions (see [50] for a detailed discussion) beyond the capability of a human operator. This leaves the tool of ML.

ML in this context consists of employing supervised algorithm techniques to search for functional forms of the collision frequency that best fit the datasets generated by numerical inversion. The identification of this functional form can be accomplished through methods such as nearest neighbor, neural networks, and Gaussian processes. The ML we employ here is based on symbolic regression [51, 52]. This approach is distinguished from other ML techniques in that in lieu of assuming a set of base functions or imposing a model structure for the fit, symbolic regression is open-ended, systematically proposing and evaluating combinations of analytical functions for their goodness of fit to the experimental data. In this way, the algorithm ultimately yields symbolic functional forms for $\nu_{\mathrm{AN}}(T_e,\ n_e, \ldots)$. These types of expressions easily can be evaluated for new datasets to determine their predictive capability. Moreover, their expression in symbolic terms affords an opportunity for some fundamental insight—allowing us to evaluate which plasma parameters are dominant in influencing the anomalous collision frequency.

3. Implementation

The implementation of the architecture we outlined above requires two elements: the generation of training datasets and a ML algorithm to search for the functional form of the frequency.

3.1. Generation of datasets

We employed in this work the results of Hall2De, a numerical Hall thruster code developed at the NASA Jet Propulsion Laboratory (JPL) [17], to provide datasets of the empirically-determined anomalous collision frequency in a set of Hall thrusters. Hall2De is a 2D, r-z, multi-fluid solver that concurrently evaluates fluid equations for electrons and multiple ion fluids (demarcated by the charge state and location). The neutrals are propagated in the geometry with a line-of-sight algorithm. Hall2De solves the fluid equations by decomposing them into components parallel and perpendicular to a magnetic field aligned mesh. The input and boundary conditions to the code include the geometry, magnetic field topography, discharge voltage, and flow rate. The discharge current, thruster, and plasma parameters as a function of position are the primary outputs.

Hall2De can be used to infer the anomalous collision frequency in an experimentally-characterized Hall thruster per the numerical inversion method discussed in section 2.3. In this code, however, instead of specifying the value for the anomalous collision frequency at each point in the simulation grid independently, the user only inputs the guess for the anomalous collision frequency values along the channel centerline of the thruster, $\nu_{AN}|_{CL}$. These values are then mapped to the rest of the thruster by projecting them along their respective magnetic fields and scaling by the magnitude of the field $\nu_{AN}(B) = (B/B_{CL})\, \nu_{AN}|_{CL}$. The code is run to convergence with these specified values of collision frequency. The goodness of the guess for the collision frequency profile is then benchmarked by comparing the outputs for Hall2De to experimental measurements of the discharge current and thrust as well as local plasma measurements including the electron temperature profile along centerline, the plasma potential along centerline, and the axial ion velocity. These latter measurements are informed by probe- and laser-based techniques for measuring the plasma (see [53, 54]). Using the numerical inversion technique, Hall2De has been shown to yield numerical results that are quantitatively consistent with many aspects of experimentally-measured thrusters (see [49, 55, 56]). Moreover, the empirically determined collision frequency profiles found with this technique exhibit qualitatively and quantitatively similar features to the profiles that actually have been measured with direct probing techniques (compare, e.g. figure 5 from [44] and figure 8 in this work).

We employed Hall2De's experimentally derived anomalous collision frequency from nine operating conditions for four different Hall thrusters. These datasets were provided by JPL and included data on the H6US [57–59], a 6 kW laboratory thruster that was the result of a joint development between the Air Force Research Laboratory, JPL, and the University of Michigan; the H6MS [56, 60], a version of the H6US that was designed by JPL which modified the magnetic topography to be magnetically shielded; and two commercial systems, denoted here as Commercial Hall Thruster I and Commercial Hall Thruster II. All four of these thrusters broadly speaking follow the optimized, empirical scaling laws that have informed state of the art, moderate-power (1–5 kW) Hall thruster design in the past three decades (see [61]). They all are intended to operate between 1 and 6 kW with similar in-channel current densities and channel width to thruster radius ratios. Xenon was the working gas for all four systems, and for the nine operating conditions, flow rates varied from 5 to 25 mg s^{-1} with the standard cathode flow fraction of 7% and discharge voltages of 300 and 400 V. Key differences between the thrusters include the magnetic field topography (shielded versus unshielded), cathode geometry and location (externally mounted vs internally mounted), and thruster materials. The general purpose behind employing four modern but disparate systems was to provide a diverse dataset (i.e. to not bias it toward one thruster over another) while still representing technologies that are relevant and in use.

For each thruster configuration, we note that while Hall2De was capable of generating two-dimensional datasets over the entire simulated domain, the assumed dependency of the anomalous collision frequency off centerline makes these off-axis points non-unique (see [50] for additional discussion). Therefore, for this investigation we only extracted numerical data along the channel centerline of each simulated thruster. Moreover, to provide uniformity across the different datasets (despite employing different geometries and meshes), we interpolated the numerical data results from each dataset along the channel centerline and sampled these interpolations into 100 equally spaced points in the axial direction. For each case, the Hall2De simulations considered the electrons, neutrals, and three species of ions and ion charge states. Each data point extracted from the numerical code included ~30 local plasma parameters and 20 calculated collision frequencies.

While this wide parameter space could, in principle, be regressed with a powerful ML algorithm, the large number of independent variables ultimately would lead to results that are too convolved to interpret. Moreover, the symbolic regression we apply to this system has no way of differentiating units or dimensions. Thus, if applied directly to the dataset, it would yield analytical expressions with dimensions that may not match collision frequency. In order to simplify our search, we narrowed our parameter space in two ways. First, we only considered characteristic velocities, lengths, and frequencies in the dataset. This choice largely was driven by physical intuition and is consistent with most first-principles models proposed to date. Second, we normalized each of these plasma properties by a characteristic value. The advantages of this normalization are that it serves to scale all the input parameters to a common range and it allows us to reduce the parameter space of independent variables (thereby easing the requirements on the regression algorithm). The independent

Table 2. Normalized plasma parameters employed as independent variables in regression model.

Frequencies normalized by electron cyclotron frequency, ω_{ce}	
Ion plasma frequency	ω_{pi}
Classical electron collision frequency	f_e
Singly-charged, classical ion collision frequency	f_i
Velocities normalized by ion sound speed, c_s	
Singly-charged ion axial velocity	u_i
Electron Hall velocity	v_{de}
Length scales normalized by electron Larmor radius, r_{ce}	
Debye length	λ_{de}
Pressure gradient length-scale	$L_P = P_e/\nabla P_e$
Ion drift velocity length-scale	$L_{ui} = u_i/\nabla u_i$

variables we included in the simulation along with the normalization parameters are shown in table 2.

3.2. Symbolic regression

We employed the commercially available DataModeler from Evolved Analytics on the Mathematica platform for this study. This symbolic regression code leverages an evolutionary, genetic algorithm to propose, iterate, and refine candidate analytical functions to fit training datasets. The user inputs a dependent variable—in this case the normalized anomalous collision frequency, ν_{AN}/ω_{ce}—and the other plasma parameters as independent variables (table 2). The user similarly selects possible operator building blocks for functions. Examples include addition, subtraction, multiplication, and square roots. The algorithm begins by randomly sampling different function combinations of the dependent variables and evaluating the goodness of fit of these functions to the data. For DataModeler, the metric for goodness of fit is given by $1 - R^2$, where R^2 is the coefficient of determination. Formally, this value is the ratio of the residual sum of squares to the square of the variance of the data: $1 - R^2 = \sum_i(\nu_{AN(i)} - f_{(i)})^2/\sum_i(\nu_{AN(i)} - \overline{\nu}_{AN})^2$, where $\nu_{AN(i)}$ denotes the ith element of the anomalous collision frequency from the dataset, $f_{(i)}$ denotes the regression model prediction for that anomalous collision frequency, and $\overline{\nu}_{AN}$ denotes the average of the anomalous collision frequency over the dataset. In the context of interpreting this parameter in terms of a model's goodness of fit, the numerator is the total error associated with a given model proposed by the algorithm. The denominator is the error from a model that assumes the functional form for the anomalous collision frequency is a constant given by the average value of the dataset, $f_{(i)} = \overline{\nu}_{AN}$. From this definition, it can be seen that $1 - R^2 \geqslant 0$ and that this parameter also can exceed 1 ($1 - R^2 > 1$). Physically, this latter case corresponds to a proposed model that is less adept at predicting the anomalous collision frequency than simply assuming a constant value given by the average of the data. As a rule, lower values of $1 - R^2$ correspond to better fits with the data.

Employing this metric for the goodness of fit, the symbolic algorithm then evolves by selecting certain base functions and dismissing others, ultimately advancing through mutation and cross-over through multiple generations in an effort to minimize the error function. The output of the algorithm consists of a number of candidate functional models that are ranked by the goodness of fit and complexity. Complexity in this case is governed by the number of terms that appear in the resulting analytical expression and the operators employed. Basic algebraic operations have the lowest complexity while transcendental functions have the highest. The results are expressed as Pareto charts of the different models wherein the goodness of fit is plotted against complexity. DataModeler also has several other diagnostic features. These include the ability to assess the frequency at which each dependent parameter appears in the generated models as well as the ability to identify the most common functional combinations of these parameters. We leveraged both of these features in our analysis.

4. Results

We first present here the driven models for the anomalous collision (section 4.1) found by applying symbolic regression to a 'training' dataset. This dataset includes the H6US, H6MS, and Commercial Hall Thruster I operating at discharge voltages of 300 and 400 V and power levels varying from 3 to 6 kW. We then apply these data-driven models to predict the collision frequency (section 4.2) for a 'test' dataset that consists of values from the Commercial Hall Thruster II. We conclude by comparing the performance of the data-driven models to those that have been proposed from first-principles analysis (section 4.3).

4.1. Functional form from training data

Figure 4 shows the Pareto front for the 1000 'best-fit' models generated by applying the symbolic regression algorithm to the training dataset. Each point in this graph represents a model along with its complexity and goodness of fit. This figure also exhibits a characteristic Pareto front 'knee' that illustrates an effective inflection point between model complexity and accuracy. Models with lower complexity than this knee do not predict behavior well (high $1 - R^2$). Models with higher complexity yield expressions that overfit the data. The optimal models from the regression generally are drawn from this knee.

We show in table 3 functional forms for three representative models from the Pareto knee. This table also lists the relative complexity of each expression as well as the goodness of fit of the functions. We thus can see explicitly the trade between the accuracy and number of terms. In all three cases, we emphasize that we did not pre-select the base functions in these expressions—they were determined by the algorithm. The physical meaning of the values of the numerical coefficients for these functions is difficult to interpret as they are the result of minimizing the residual of error when applied to the data. Of more physical significance, however, is

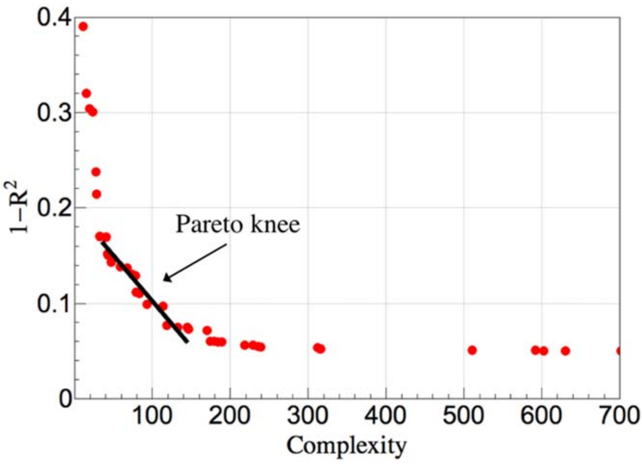

Figure 4. Pareto front plot of the results of the machine learning symbolic regression.

that all of these models depend on common plasma parameters including both the ion axial drift velocity and the electron drift velocity in the Hall direction. This observation is consistent with nearly all of the models identified with the regression algorithm. We reserve a discussion of these dependencies for section 5 and for now focus on the quantitative performance of each of these models in matching the training data.

To this end, we show in figure 5(a) the normalized anomalous collision frequency values determined from three Pareto knee models (table 3) compared to the actual values from one of the thrusters in the training dataset, the H6US at 300 V and 6 kW. We plot the collision frequency as a function of axial position along the thruster channel centerline (expressed in arbitrary units) for illustrative purposes. Though, we note that in practice each data-driven model did not take spatial position into account (table 3). They only used the plasma parameters from the Hall2De dataset outlined in table 2 from each location along centerline as inputs. With this in mind, the close correspondence between the data-driven model and the dataset on centerline in figure 5(a) serves as an initial validation of the ability of the regression algorithm to generate analytical functions that can match the training data with a high degree of fidelity. This would seem to suggest that at least for known datasets, data-driven methods are a viable method for generating closure.

4.2. Predictive capability

To investigate the predictive capability of the data-driven models, we applied the results (table 3) that emerged from our symbolic regression to the 'test' dataset from a *completely different* thruster than the three used in the 'training' dataset, namely Commercial Hall thruster II. The operating condition in this case was 300 V and 4.5 kW. We show these results in figure 5(b). Here we again have chosen to make the dependent axis the axial location in the thruster but emphasize that this parameter does not factor into the model's evaluation of the collision frequency. It is rather informed by the local plasma conditions (table 2) at each point.

From this plot, we can see that for all three models, there is marked agreement with data downstream of a minimum point (at axial location of 10) where they each capture quantitatively a similar exponential rise in normalized collision frequency. Moreover, all the models appear to show, at least in some measure, the inflection point in the upstream region. A similar inflection point did not appear in our training data profile shown in figure 5(b). Yet, all three of the data-driven models approximate it. In other words, these models are able to predict features that change between the training and the test datasets. This result thus serves to show that not only can the data-driven models match the measurements that informed them but that they can be extended to new datasets with a measure of predictive capability. As we discuss further in section 5, it is important to caveat this remark with the understanding that although the data-driven model demonstrates a predictive capability on a different thruster than used in the training dataset, this thruster leverages similar design principles and operating conditions as the thrusters in the training dataset. This new thruster's plasma properties and electron transport thus are also expected to be comparable to that of the devices that comprised the training dataset. The agreement between model and result, while marked, is not unexpected.

4.3. Comparison to first-principles models

We contrast here the results of our data-driven model with the first-principles closures that have been proposed to date (table 1). To this end, we consider both the training (section 4.1) and test datasets (section 4.2). In order to provide the best representation for each first-principles model, we first determined the values of the free parameters (e.g. the constant K) that yielded the best fits to the training data set. The results for these fit parameters are listed in table 4.

Armed with these results, we show in figure 6 response plots to the training dataset of both the first-principles models and one of the data-driven models (Model III). These figures plot the observed anomalous collision frequency from the datasets (normalized) as the independent variable and the predictions from the functional model as the dependent variable. A perfect model would fall along the drawn solid lines. It is evident from all of these results that the first-principles closures do not exhibit the same fidelity as the data-driven model (figure 6(f)). Some appear anti-correlated with the data (figures 6(a) and (b)), while others are scattered or only qualitatively predict the measured values. The closest approximations are the Turbulence II and III models which illustrate the correct general trends. In contrast, the data-driven model not only captures the qualitative trends but generally shows quantitative agreement over the nearly four orders of magnitude spanned by the dataset. We further comment that although we only show one case here for illustrative purposes, the other models from table 3 (I and II) exhibited similar response curves.

Table 3. Three of the functional forms identified from symbolic regression drawn from the Pareto knee in figure 4.

Data-driven model	Functional form	Complexity	$1 - R^2$
I	$\omega_{ce}\left(-3.37 \times 10^{-2} + \dfrac{2.39u_i}{3.32c_s + v_{de}}\right)$	28	0.22
II	$\omega_{ce}\left(1.67 \times 10^{-2} - 0.31\dfrac{\lambda_{de}}{r_{ce}} + \dfrac{0.39u_i^2}{c_s(5.89c_s + v_{de})}\right)$	40	0.17
III	$\omega_{ce}\left(6.90 \times 10^{-4} + \dfrac{14.55u_i^2}{503c_s^2 + v_{de}c_s + v_{de}^2}\right)$	43	0.15

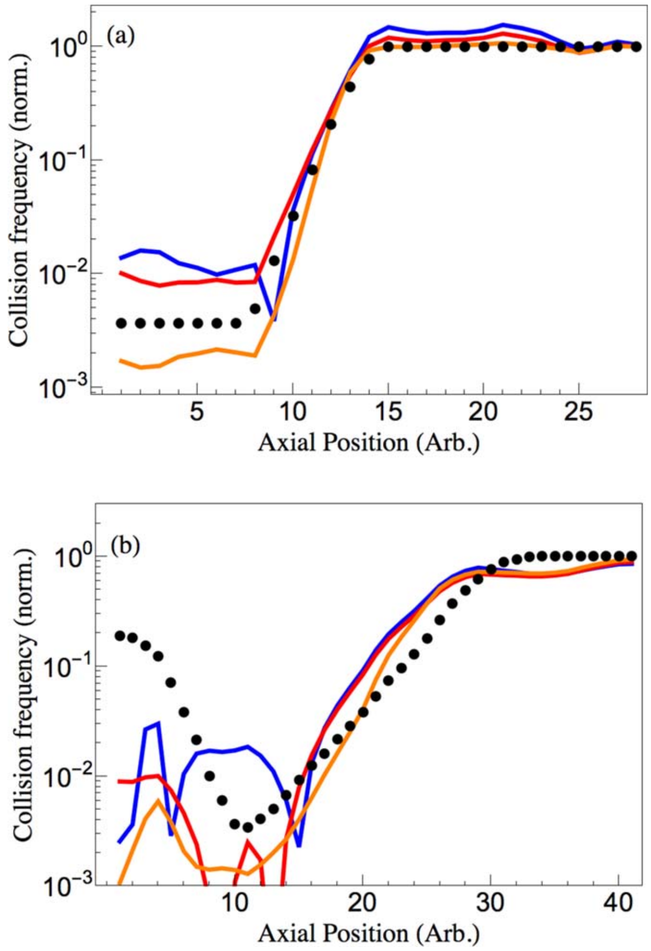

Figure 5. Normalized anomalous collision frequency profile (data points) along channel centerline for the (a) H6US at 300 V and 6 kW from the training dataset and (b) Commercial Hall thruster II at 300 V and 4.5 kW from the test dataset. The three solid curves are the results of data-driven Model I (red), Model II (blue) and Model III (orange) drawn from table 3 when applied to the datasets.

We can quantify these qualitative observations from the response plots by converting them into $1 - R^2$ values for each model. These are shown as the gray bars in figure 7. For comparison, we also show as a dotted line in this plot the value of $R^2 = 0$. A model with this coefficient of determination (section 3.2) is functionally the equivalent of using the mean of the training dataset as the model for the anomalous collision frequency. Models with $1 - R^2 > 1$ thus offer no improvement in predictive capability over using a constant, average value. With this in mind, we now can see that the trends we noted in figure 6 are supported by the coefficient of determination analysis in figure 7. Indeed, the Turbulence II, III, and data-driven models yield the best agreement with the training dataset. Of all the first-principles closures, however, only the Turbulence III model has $1 - R^2 < 1$. The data-driven model exhibits the least error compared to the other closures.

Table 4. Best fit parameters to training dataset for the first-principles models.

Mechanism	Best fit parameter
Wall collisions	$K = 2000$
Turbulence I	$K = 29$
Turbulence II	$K = 1.3$; $C = 3.6 \times 10^{-8}$; $\alpha = 1$
Turbulence III	$K = 23$

It ultimately is not surprising that the data-driven model exhibits better agreement with the training data than the other closures. It is based on using numerical tools to fit this specific dataset. The more objective comparison is to apply the models to the test dataset that was not used in the regression. To this end, we also show in figure 7 in blue the $1 - R^2$ values for the different models as evaluated on the data from Commercial Hall thruster II. It immediately emerges from this result that the trends are both quantitatively and qualitatively the same as with the training data. The data-driven model ultimately exhibits a better ability than the other first-principles closures to match the collision frequency values.

As a final metric, we show in figure the same test dataset from figure 5(b) along thruster centerline compared with the predictions from the data-driven model III and the two first-principles models, Turbulence II and III, that showed the best agreement with the data. Here we can see that both of the first-principles models exhibit qualitatively correct trends—capturing the effective inflection point—but that quantitatively they have orders of magnitude discrepancies with the data. In contrast, the data-driven functional model recreates both quantitatively and qualitatively the correct behavior. We note compared to the other two models, the data-driven model III does underestimate the anomalous collision frequency upstream of the inflection (0–10 position). However, it has been found [30, 50] that in this region Hall2De's estimates for the anomalous collision frequency can be to some extent arbitrary. Classical collisions are the dominant effect here, so

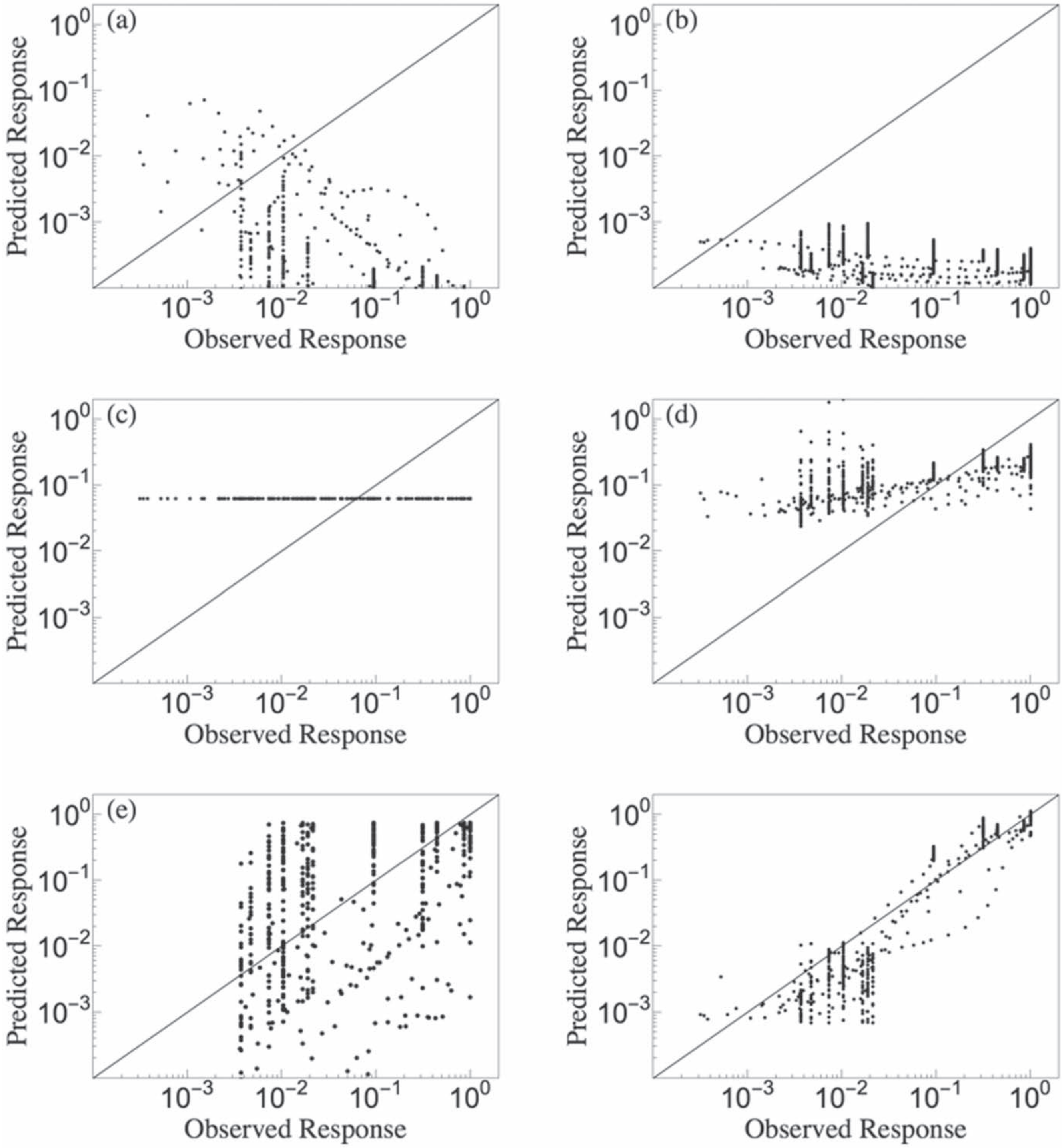

Figure 6. Response plots for anomalous collision frequency models drawn from the training data set for the (a) Wall model, (b) Turbulence I model, (c) Bohm model, (d) Turbulence II model, (e) Turbulence III model, and (f) Data-driven model III.

the values for the anomalous collision frequency in this region are ambiguous at best. As a result, both the training dataset and the subsequent model results in this region are not as critical to modeling thruster behavior. With this in mind, we see that the ML approach has a substantially higher degree of agreement with the data than the first-principles models in the more physical, downstream regions. In the following section, we discuss the implications of this finding.

5. Discussion

Our results have demonstrated not only the ability of data-driven functions for the anomalous collision frequency to match training sets but also to predict—in some measure—the functional dependence of the anomalous collision frequency on plasma properties in a completely different thruster. We also have showed quantitatively the ability of these

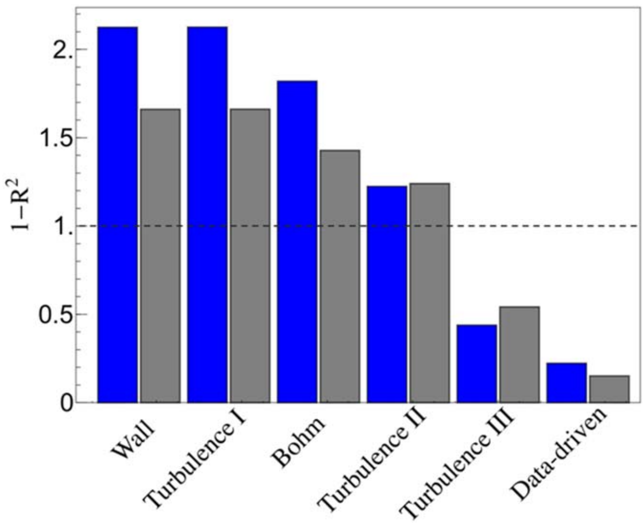

Figure 7. $1 - R^2$ values for different closures. Gray denotes the training data set and blue is from the test data set. The dotted line corresponds to a model based on using the mean value of collision frequency from the training dataset.

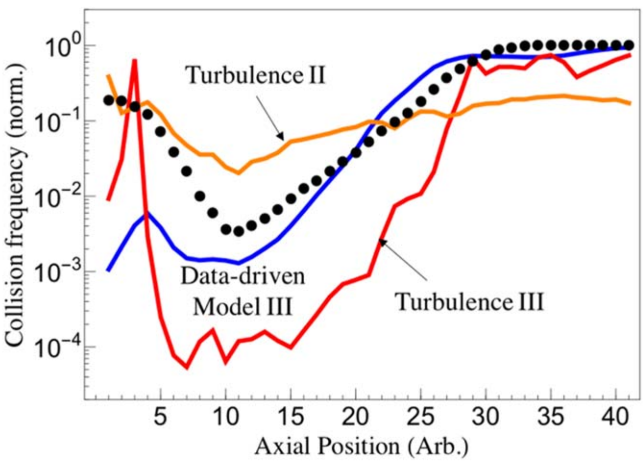

Figure 8. Predictions (solid lines) for the anomalous collision frequency according to three models along centerline compared to the test dataset from Commercial Hall Thruster II at 300 V and 4.5 kW (points).

data-driven models to provide better agreement with data than existing models derived from first-principles. With these observations in mind, we discuss here some caveats to these findings as well as potential physical insight yielded by this work.

From the perspective of physical significance, the fact that our regression technique is symbolic affords us an opportunity to examine the generated models for insight into what physical processes may be driving the anomalous mechanism for transport. For example, we show in figure 9 a plot of the frequency of each normalized variable's appearance (table 2) in all the best-fit models generated by the regression algorithm. This is a quantitative assessment of how 'important' each variable is for a model to fit the data. What immediately appears from this figure—and is consistent with the sample models we showed in table 3—is that two

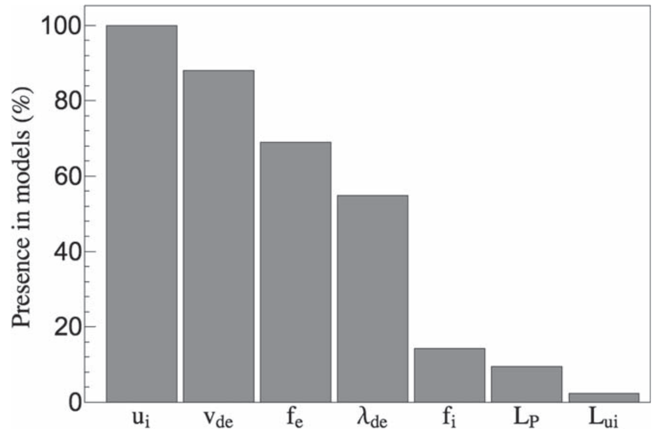

Figure 9. Percentage of models from the Pareto front in figure 4 that incorporate the shown normalized parameter. Plasma frequency did not appear in the models.

dominant contributors are the ion drift velocity and the electron Hall drift velocity (normalized by ion sound speed). We can interpret the predominance of these two variables through the framework of one of the leading theories proposed to date for the explanation of anomalous transport: the onset of current-driven turbulence.

In this context, the dependence of the models on the electron drift is not surprising given that the Hall effect current is the driving source for the onset of this turbulence. The importance of the second variable, the ion drift speed, is less evident from the interpretation of turbulence as a driving factor. One possibility, as others have pointed to, is that the ion drift may play a role in balancing the growth of the turbulent energy [30, 34, 62]. As an additional guidepost for an analytical, first-principles investigation, we also were able to establish functionally how these dominant contributors to the data-driven models combine to yield the best match with experimental data. From a correlation analysis of the models from the Pareto front in figure 4, we find that the most common functional combination of variables is given as

$$\nu_{\rm AN} \propto \omega_{ce}\left(\frac{u_i}{\mathrm{v}_{de}}\right)^2. \tag{5}$$

The physical origin of this result is not immediately apparent. However, it does appear to suggest the collision frequency may be Bohm-like though modified by a corrective term that depends on the ratio of ion to electron drift velocities.

In addition to pointing to two dominant parameters correlated with the anomalous collision frequency, this work allows us to evaluate the relative unimportance of other factors. In particular, we can see from figure 9 that classical ion collisions as well as the gradients for both pressure and ion drift do not appear in a high fraction of models. This suggests that physically these inputs may not be dominant drivers in the fluid-formulation for the anomalous collision frequency. This stands in contrast to some of the first-principles models outlined in table 2. As for the other parameters with intermediate presence in the best models such as the electron collision frequency and Debye length, their appearance at a rate of 50% suggests that they may have some weaker role. However, it is not immediately evident if and how. Additional simulations with protracted run times may help identify the relative importance of these parameters. With that said, we ultimately recognize that data-driven results may never lead to a direct, fundamental conclusion about the underlying physics. Rather, from the perspective of first principles insight, the major contribution from regression work is that it provides us with a new tool for inspiring hypotheses for the physics of the anomalous term.

Leaving aside the physical interpretation of these results, there are a few caveats to this analysis that we mention here. The first is that our functional forms from the ML technique are not perfect and in fact exhibit marked deviations even from the training datasets (figures 5 and 6(e)). While this is a sign that we are not overfitting the data, it does call into question the extensibility of this model to parameter regimes that are significantly outside those modeled here. It remains to be seen how well the model works for off-nominal operating conditions. Indeed, although we demonstrated the predictive capability of this model by applying it to a different thruster geometry than those used for training, it is important to note that all the thrusters considered in this work rely on similar design principles (section 3.1) and operate over a narrow envelope of canonical conditions for these devices (300–400 V and 1–6 kW). The notable success of the predictive ability of this model to match a different thruster configuration (section 4.2) thus may largely stem from the fact that this device was not substantially different in design than the other thrusters. As a follow-on consideration to this, one of the major challenges of this approach is that there is not a unique model that best fits the data. As Table 3 shows, there are multiple candidate functional expressions exhibiting different dependencies on the plasma parameters. While all of these ultimately show similar goodness of fits, their degeneracy complicates efforts to intuit the underlying physics from these models or to determine which one best will predict the collision frequency for a new thruster geometry. As with all data-driven algorithms, these challenges may in part be addressed by increasing the number of thrusters and operating conditions included in the datasets.

As a second concern, all of this work to date has been on existing datasets, both for training and testing. We have applied ML regression to see if there are functional forms that fit this data. We have yet to incorporate self-consistently the closures identified by the ML algorithmic into a thruster code. These numerical models, when self-consistently evaluated with the functional forms we identified in table 3, may prove to yield anomalous collision frequency profiles that differ than the shapes shown here. Or, in the extreme case, may not yield unique or convergent solutions at all. This will be the ultimate test of the predictive capability of this model.

For a third caveat, we raise the larger question as to the validity of the approximation that the anomalous effects in the plume can be represtend as an effective scalar collision frequency (equation (3)). Indeed, it is not immediately evident if this formulation is correct. For example, the anomalous effects may be anisotropic in the plume, thus requiring a tensor formulation. Or, we recognize the possibility that approximating the effects of whatever mechanism drives the turbulence with fluid equations may not even be valid [63]. The search for a functional form, even aided by data-driven techniques, thus may be limited as to the insight it can yield. With that said, our work to date does seem to suggest that there are at least some functional forms based on fluid properties that fit the data. Indeed, the positive results we have presented here indicate that a data-driven approach may be an effective and novel tool for approaching the problem of electron transport.

6. Conclusions

We have explored in this work the application of data-driven techniques with ML for the purpose of investigating the problem of anomalous electron transport in Hall effect thrusters. Following a standard approach in the community, we have couched this problem in terms of a fluid formulation where we have related the cross-field transport with an effective anomalous electron collision frequency. In so doing, the problem was reduced to finding a self-consistent expression for the scalar anomalous collision frequency that depends on the background fluid properties. While there have been a number of attempts at identifying this form from first-principles, in this work we have applied a data-driven approach. We employed seven datasets from three state of the art Hall thrusters generated from the empirically validated fluid-code Hall2De to train a ML algorithm based on symbolic regression. We showed that the analysis of these datasets yielded a functional form of the anomalous collision frequency that matched the experimental measurements. Moreover, we demonstrated that this functional form was extensible beyond the training dataset. In particular, we were able to use our result to predict qualitative and quantitative trends in the anomalous collision frequency for a thruster geometry not included in our training data. We similarly showed that the data-driven model for this case exhibited better agreement with the anomalous collision than the preditions from five existing closure models derived from first-principles. In addition to demonstrating this predictive capability, we leveraged the symbolic regression method in this work to generate potential physical insight into the processes governing the anomalous transport. It emerged from this analysis that both the electron Hall drift and ion drift speed may have dominant roles in governing the anomalous collision frequency. We similarly have conjectured about the reason why these dependencies exist—primarily through the interpretation that the collision frequency results from turbulence in the plasma. We have discussed the limitations of this approach both in terms of the validity of attempting to approximate kinetic effects with a fluid approximation as well as the challenges with extending a data-driven model to off-nominal configurations. Despite these issues, we believe that the results here have demonstrated the promise of data-driven modeling as a tool for addressing the problem of electron transport. Indeed, this approach may even offer a path toward achieving the ultimate goal of a Hall thruster code with a predictive capability.

Acknowledgements

The author would like to acknowledge Dr Ioannis Mikellides and Dr Alejandro Lopez-Ortega of the NASA Jet Propulsion Laboratory for providing the Hall2De simulation results. The author also would like to thank Prof Karthik Duraisamy from the University of Michigan for fruitful discussions on the problems of closure and the promise of machine learning. He simlarly would like to express his gratitude to Mr. Marcel Georgin, Ms. Angela Kimber, and Mr. Ethan Dale for their comments and feedback on the manuscript.

ORCID iDs

Benjamin Jorns https://orcid.org/0000-0001-9296-2044

References

[1] Boeuf J-P 2017 Tutorial: physics and modeling of Hall thrusters *J. Appl. Phys.* **121** 11101
[2] Héron A and Adam J C 2013 Anomalous conductivity in Hall thrusters: effects of the non-linear coupling of the electron-cyclotron drift instability with secondary electron emission of the walls *Phys. Plasmas* **20** 82313
[3] Boeuf J-P and Chaudhury B 2013 Rotating instability in low-temperature magnetized plasmas *Phys. Rev. Lett.* **111** 155005
[4] Tang D L, Geng S F, Qiu X M and Chu P K 2012 Three-dimensional numerical investigation of electron transport with rotating spoke in a cylindrical anode layer Hall plasma accelerator *Phys. Plasmas* **19** 073519
[5] Taccogna F, Schneider R, Longo S and Capitelli M 2008 Kinetic simulations of a plasma thruster *Plasma Sources Sci. Technol.* **17** 024003
[6] Matyash K, Schneider R, Mazouffre S, Tsikata S and Grimaud L 2017 Investigation of rotating spoke instabilities in a wall-less Hall thruster: II. Simulation *Proc. 35th Int. Electric Propulsion Conf.* IEPC-2017-403
[7] Cho S *et al* 2015 Study of electron transport in a Hall thruster by axial-radial fully kinetic particle simulation *Phys. Plasmas* **22** 103523
[8] Fife J M and Martinez-Sanchez M 1995 Two-dimensional hybrid particle-in-cell (PIC) modeling of Hall thrusters *Proc. 24th Int. Electric Propulsion Conf.* IEPC-95-24
[9] Parra F I, Ahedo E, Fife J M and Martínez-Sánchez M 2006 A two-dimensional hybrid model of the Hall thruster discharge *J. Appl. Phys.* **100** 23304
[10] Koo J W and Boyd I D 2004 Computational model of a Hall thruster *Comput. Phys. Commun.* **164** 442–7
[11] Hofer R *et al* 2008 Efficacy of electron mobility models in hybrid-PIC Hall thruster simulations *Proc. 44th AIAA Joint Propulsion Conf.* AIAA-2008-4924
[12] Bareilles J, Hagelaar G J M, Garrigues L, Boniface C, Boeuf J P and Gascon N 2004 Critical assessment of a two-dimensional hybrid Hall thruster model: comparisons with experiments *Phys. Plasmas* **11** 3035–46
[13] Hagelaar G J M, Bareilles J, Garrigues L and Boeuf J-P 2003 Role of anomalous electron transport in a stationary plasma thruster simulation *J. Appl. Phys.* **93** 67–75
[14] Hara K and Boyd I D 2015 Axial-azimuthal hybrid-direct kinetic simulation of Hall effect thrusters *Proc. 34th Int. Electric Propuls* IEPC-2015-286
[15] Kawashima R, Hara K and Komurasaki K 2018 Numerical analysis of azimuthal rotating spokes in a crossed-field discharge plasma *Plasma Sources Sci. Technol.* **27** 35010
[16] Hara K, Sekerak M J, Boyd I D and Gallimore A D 2014 Mode transition of a Hall thruster discharge plasma *J. Appl. Phys.* **115** 203304
[17] Mikellides I G and Katz I 2012 Numerical simulations of Hall-effect plasma accelerators on a magnetic-field-aligned mesh *Phys. Rev.* E **86** 1–17
[18] Adam J C, Héron A and Laval G 2004 Study of stationary plasma thrusters using two-dimensional fully kinetic simulations *Phys. Plasmas* **11** 295–305
[19] Ducrocq A, Adam J C, Ήron A and Laval G 2006 High-frequency electron drift instability in the cross-field configuration of Hall thrusters *Phys. Plasmas* **13** 102111
[20] Lazurenko A, Krasnoselskikh V and Bouchoule A 2008 Experimental insights into high-frequency instabilities and related anomalous electron transport in Hall thrusters *IEEE Trans. Plasma Sci.* **36** 1977–88
[21] Tsikata S, Lemoine N, Pisarev V and Gfsillon D M 2009 Dispersion relations of electron density fluctuations in a Hall thruster plasma, observed by collective light scattering *Phys. Plasmas* **16** 033506
[22] Brown Z A and Jorns B A 2017 Dispersion relation measurements of plasma modes in the near-field plume of a 9 kW magnetically shielded thruster *Proc. 35th Int. Electric Propulsion Conf.* IEPC-2017-387
[23] Gascon N, Dudeck M and Barral S 2003 Wall material effects in stationary plasma thrusters: I. Parametric studies of an SPT-100 *Phys. Plasmas* **10** 4123–36
[24] Kaganovich I D, Raitses Y, Sydorenko D and Smolyakov A 2007 Kinetic effects in a Hall thruster discharge *Phys. Plasmas* **14** 57104
[25] Mcdonald M S and Gallimore A D 2011 Rotating spoke instabilities in Hall thrusters *IEEE Trans. Plasma Sci.* **39** 2952–3
[26] Ellison C L, Raitses Y and Fisch N J 2012 Cross-field electron transport induced by a rotating spoke in a cylindrical Hall thruster *Phys. Plasmas* **013503** 1–7
[27] Cappelli M, Cha E and Fernandez E 2013 Entropy closure model for transport in Hall thruster simulations *Proc. 35th Int. Electric Propulsion Conf.* IEPC-2013-088
[28] Cappelli M A, Young C V, Cha E and Fernandez E 2015 A zero-equation turbulence model for two-dimensional hybrid Hall thruster simulations *Phys. Plasmas* **22** 114505
[29] Lafleur T, Baalrud S D and Chabert P 2017 Theory for the anomalous electron transport in Hall effect thrusters: II. Kinetic model *Phys. Plasmas* **23** 053503
[30] Mikellides I G, Ortega A L, Katz I and Jorns B A 2016 Hall2De simulations with a first-principles electron transport model based on the electron cyclotron drift instability *Proc. 52nd AIAA Joint Propulsion Conf.* AIAA-2016-4618
[31] Koo J W and Boyd I D 2006 Modeling of anomalous electron mobility in Hall thrusters *Phys. Plasmas* **13** 033501
[32] Parish E J and Duraisamy K 2016 A paradigm for data-driven predictive modeling using field inversion and machine learning *J. Comput. Phys.* **305** 758–74
[33] Singh A P, Medida S and Duraisamy K 2017 Machine learning-augmented predictive modeling of turbulent separated flows over airfoils *AIAA J.* **55** 2215–27
[34] Katz I, Lopez Ortega A, Jorns B A and Mikellides I G 2016 Growth and saturation of ion acoustic waves in hall thrusters *Proc. 52nd AIAA Joint Propulsion Conf.* AIAA-2016-4534

[35] Morozov A I and Savelyev V V 2000 Fundamentals of stationary plasma thruster theory *Reviews of Plasma Physics* ed B B Kadomtsev and V D Shafranov (Boston, MA: Springer US) pp 203–391
[36] Barral S, Makowski K, Peradzyński Z, Gascon N and Dudeck M 2003 Wall material effects in stationary plasma thrusters: II. Near-wall and in-wall conductivity *Phys. Plasmas* **10** 4137–52
[37] Garrigues L, Hagelaar G J M, Boniface C and Boeuf J P 2006 Anomalous conductivity and secondary electron emission in Hall effect thrusters *J. Appl. Phys.* **100** 123301
[38] Scharfe M K, Thomas C A, Scharfe D B, Gascon N, Cappelli M A and Fernandez E 2007 Shear-based model for electron transport in 2D hybrid Hall thruster simulations *IEEE Trans. Plasma Sci.* **36** 2058–68
[39] Katz I, Mikellides I G, Jorns B A and Ortega A L 2015 Hall2De simulations with an anomalous transport model *Proc. 34th Int. Electric Propulsion Conf.* IEPC-2015-402
[40] Ahedo E, Gallardo J M and Martínez-Sánchez M 2003 Effects of the radial plasma-wall interaction on the Hall thruster discharge *Phys. Plasmas* **10** 3397–409
[41] Lafleur T, Baalrud S D and Chabert P 2016 Theory for the anomalous electron transport in Hall effect thrusters: I. Insights from particle-in-cell simulations *Phys. Plasmas* **23** 053502
[42] Reza M, Faraji F, Andreussi T and Andrenucci M 2017 A model for turbulence-induced electron transport in Hall thrusters *Proc. 34th Int. Electric Propulsion Conf.* IEPC-2017-367
[43] Boniface C, Garrigues L, Hagelaar G J M, Boeuf J P, Gawron D and Mazouffre S 2006 Anomalous cross field electron transport in a Hall effect thruster *Appl. Phys. Lett.* **89** 161503
[44] Linnell J A and Gallimore A D 2009 Hall thruster electron motion characterization based on internal probe measurements *Proc. 31st Int. Electric Propulsion Conf.* 2009–105
[45] Durot C J, Jorns B A, Dale E T and Gallimore A D 2017 Laser-induced fluorescence measurement of the anomalous collision frequency in a 9 kW magnetically-shielded Hall thruster *Proc. 35th Int. Electr. Propuls. Conf.* IEPC-2017-029
[46] Meezan N B, Hargus W A and Cappelli M A 2001 Anomalous electron mobility in a coaxial Hall discharge plasma *Phys. Rev.* E **63** 026410
[47] Jorns B A, Hofer R H and Mikellides I G 2014 Power dependence of the electron anomalous collision frequency in a Hall thruster *Proc. 50th AIAA Joint Propulsion Conf.* (https://doi.org/10.2514/6.2014-3620)
[48] Garrigues L, rez-Luna J, Lo J, Hagelaar G J M, Boeuf J P and Mazouffre S 2009 Empirical electron cross-field mobility in a Hall effect thruster *Appl. Phys. Lett.* **95** 41501
[49] Lopez Ortega A, Mikellides I and Chaplin V 2017 Numerical simulations for the assessment of erosion in the 12.5 kW Hall effect rocket with magnetic shielding (HERMeS) *Proc. 35th Int. Electric Propulsion Conf.* IEPC-2017-154
[50] Mikellides I and Lopez-Ortega A 2018 Challenges in the development and verification of first principles models of the anomalous transport in Hall-effect thrusters *Plasma Sources Sci. Technol.* accepted http://iopscience.iop.org/article/10.1088/1361-6595/aae63b
[51] Kotanchek M, Smits G and Vladislavleva E 2008 Trustable symbolic regression models: using ensembles, interval arithmetic and pareto fronts to develop robust and trust-aware models *Genetic Programming Theory and Practice V* ed R Riolo *et al* (Boston, MA: Springer US) 201–20
[52] Riolo R, Vladislavleva E and Moore J H 2011 *Genetic Programming Theory and Practice IX* (New York: Springer)
[53] Jorns B *et al* 2016 Mechanisms for pole piece erosion in a 6 kW magnetically-shielded Hall thruster *Proc. 52nd AIAA Joint Propulsion Conf.* AIAA-2016-4839 (https://doi.org/10.2514/6.2016-4839)
[54] Chaplin V *et al* 2017 Laser-induced fluorescence measurements of the acceleration zone in the 12. 5 kW HERMeS Hall Thruster *Proc. 35th Int. Electric Propulsion Conf.* IEPC-2017-229
[55] Ortega A L, Jorns B A, Mikellides I G and Hofer R R 2015 Numerical simulations of the XR-5 Hall thruster for life assessment at different operating conditions *Proc. 51st AIAA Joint Propulsion Conf.* AIAA-2015-4008 (https://doi.org/10.2514/6.2015-4008)
[56] Mikellides I G, Katz I, Hofer R R and Goebel D M 2014 Magnetic shielding of a laboratory Hall thruster: I. Theory and validation *J. Appl. Phys.* **115** 043303
[57] Haas J M, Hofer R R, Brown D L, Reid B M and Gallimore A D 2007 Design of the H6 Hall thruster for high thrust/power investigation *54th JANNAF Propulsion Meeting (Denver, CO, 14–17 May)*
[58] Brown D *et al* 2007 Performance characterization and design verification of the H6 laboratory model Hall thruster *54th JANNAF Propulsion Meeting (Denver, CO, May 14–17)*
[59] Reid B, Gallimore A, Hoer R, Li Y and Haaas J 2007 Anode design and verification for the H6 Hall thruster *54th JANNAF Propulsion Meeting (Denver, CO, May 14–17)*
[60] Hofer R R, Goebel D M, Mikellides I G and Katz I 2014 Magnetic shielding of a laboratory Hall thruster: II. Experiments *J. Appl. Phys.* **115** 043304
[61] Dannenmayer K and Mazouffre S 2011 Elementary scaling relations for Hall effect thrusters *J. Propulsion Power* **27** 236–45
[62] Lafleur T, Baalrud S D and Chabert P 2016 Theory for the anomalous electron transport in Hall effect thrusters: II. Kinetic model *Phys. Plasmas* **23** 053503
[63] Lafleur T, Martorelli R, Chabert P and Bourdon A 2018 Anomalous electron transport in Hall-effect thrusters: comparison between quasi-linear kinetic theory and particle-in-cell simulations *Phys. Plasmas* **25** 061202
[64] Mikellides I G, Katz I, Hofer R R, Goebel D M, De Grys K and Mathers A 2011 Magnetic shielding of the channel walls in a Hall plasma accelerator *Phys. Plasmas* **18** 033501